ISSN 1674-1056
http://cpb.iphy.ac.cn
http://iopscience.iop.org/cpb
中国物理 B
Chinese Physics
中国物理
Chinese Physics B

Acoustic radiation force induced by two Airy-Gaussian beams on a cylindrical particle

Sha Gao(高莎), Yiwei Mao(毛一葳), Jiehui Liu(刘杰惠), Xiaozhou Liu(刘晓宙)
Citation: Chin. Phys. B . 2018, 27(1): 014302. **doi:** 10.1088/1674-1056/27/1/014302

Journal homepage: http://cpb.iphy.ac.cn; http://iopscience.iop.org/cpb

What follows is a list of articles you may be interested in

Review on second-harmonic generation of ultrasonic guided waves in solid media (I):Theoretical analyses

Wei-Bin Li(李卫彬), Ming-Xi Deng(邓明晰), Yan-Xun Xiang(项延训)
Chin. Phys. B . 2017, 26(11): 114302. **doi:** 10.1088/1674-1056/26/11/114302

Broadband acoustic focusing by symmetric Airy beams with phased arrays comprised of different numbers of cavity structures

Jiao Qian(钱姣), Bo-Yang Liu(刘博阳), Hong-Xiang Sun(孙宏祥), Shou-Qi Yuan(袁寿其), Xiao-Zhu Yu(俞笑竹)
Chin. Phys. B . 2017, 26(11):114304. **doi:** 10.1088/1674-1056/26/11/114304

Adaptive optimization on ultrasonic transmission tomography-based temperature image for biomedical treatment

Yun-Hao Zhu(朱昀浩), Jie Yuan(袁杰), Stephen Z Pinter, Oliver D Kripfgans, Qian Cheng(程茜), Xue-Ding Wang(王学鼎), Chao Tao(陶超), Xiao-Jun Liu(刘晓峻), Guan Xu(徐冠), Paul L Carson
Chin. Phys. B . 2017, 26(6): 064301. **doi:** 10.1088/1674-1056/26/6/064301

Temperature imaging with speed of ultrasonic transmission tomography for medical treatment control: A physical model-based method

Chu Zhe-Qi, Yuan Jie, Stephen Z. Pinter, Oliver D. Kripfgans, Wang Xue-Ding, Paul L. Carson, Liu Xiao-Jun
Chin. Phys. B . 2015, 24(10): 104303. **doi:** 10.1088/1674-1056/24/10/104303

Study of acoustic bubble cluster dynamics using a lattice Boltzmann model

Mahdi Daemi, Mohammad Taeibi-Rahni, Hamidreza Massah
Chin. Phys. B . 2015, 24(2): 024302. **doi:** 10.1088/1674-1056/24/2/024302

Acoustic radiation force induced by two Airy–Gaussian beams on a cylindrical particle*

Sha Gao(高莎), Yiwei Mao(毛一葳), Jiehui Liu(刘杰惠), and Xiaozhou Liu(刘晓宙)†

Key Laboratory of Modern Acoustics, Institute of Acoustics and School of Physics, Collaborative Innovation Center of Advanced Microstructures, Nanjing University, Nanjing 210093, *China*

(Received 10 July 2017; revised manuscript received 12 October 2017; published online 17 November 2017)

Based on the angular spectrum decomposition and partial-wave series expansion methods, we investigate the radiation force functions of two Airy–Gaussian (AiG) beams on a cylindrical particle and the motion trajectory of the particle. The simulations show that the particle can be pulled or propelled into either the positive or negative transverse direction by turning the phase difference between the two AiG beams appropriately; and the larger the beam widths of the two AiG beams are, the bigger the radiation force can be obtained to control the particle. In addition, the direction of the accelerated particle can be controlled while the dimensionless frequency bandwidth changes. The results indicate that the phase plays an important role in controlling the direction of the particle, which may provide a theoretical basis for the design of acoustical tweezers and the development of drug delivery.

Keywords: acoustic radiation force, two Airy–Gaussian beams, phase, beam width

PACS: 43.25.Qp, 43.35.Wa, 43.80.Gx **DOI:** 10.1088/1674-1056/27/1/014302

1. Introduction

Many scholars have investigated the acoustic radiation force, and the common beams, such as plane wave,[1,2] Gaussian beam,[3,4] focused beam,[5] and Bessel beam,[6,7] have been studied. Therefore, introducing an innovative type of beam for particle manipulation has to be taken into account. In optics, the Airy beam has drawn much attention of the researchers due to its unique properties,[8,9] which retains the shape of the intensity distribution during propagation (non-diffracting), and it can recover itself after encountering an obstacle (self-healing) and propagates along a parabolic trajectory (self-accelerating) similar to the ballistic trajectory under the effect of gravity, and there are some studies about the application of the Airy beam in the optical tweezers.[10–14] In addition, the Airy beam can also be applied to the study of the acoustical tweezers, which were investigated by Mitri in 2016.[15]

The Airy–Gaussian (AiG) beam, a generalized form of the Airy beam, has the similar propagation properties to the Airy beam: approximately non-diffracting, self-healing, and self-accelerating. The AiG beam was introduced by Bandres and Gutierrez-Vega,[16] who regarded the Airy beam[8] and the finite-energy Airy beam[17] as special cases of the AiG beam. In optics, the AiG beam has been analyzed extensively,[16,18] for example, the propagation properties of a single AiG beam in different media[19–21] and the interaction of two AiG beams in Kerr media[22] and nonlocal nonlinear media.[23] But in acoustics, there are few reports about the application of the AiG beam in particle manipulation, though Mitri has investigated the acoustical applications on a two-dimensional cylindrical particle in water[15] and an elastic medium[24] by an Airy beam. There is no investigation of the acoustic radiation force on a cylindrical particle induced by an AiG beam up to now.

The acoustic radiation forces induced by the traditional beams such as Bessel beam and Gaussian beam can accelerate the micro-particle along a straight line, while the acoustic radiation force induced by the Airy beam can pull, push, or accelerate the micro-particle along a parabolic trajectory,[15] in other words, the Airy beam not only exerts a force on the particle along its velocity direction but also exerts a force on the particle perpendicular to its velocity direction. The control of the particle under the effect of radiation force induced by acoustic beams is similar to the delivery of the drugs in the human's blood vessels. Considering the complexity of the human's blood vessels, the drugs need to be manipulated accurately in every direction. Therefore, the question is how to control the direction of an accelerated particle. In this paper, the acoustic radiation force induced by two AiG beams on a cylindrical particle is simulated and the effect of the radiation force on the direction of the accelerated particle is studied. We investigate the acoustic radiation force on a cylindrical particle immersed in water induced by two AiG beams using the angular spectrum decomposition and partial-wave series expansion methods. Most particle manipulations use surface acoustic wave devices which often deal with "acoustical sheets", i.e.,

*Project supported by the National Key R & D Program, China (Grant No. 2016YFF0203000), the National Natural Science Foundation of China (Grant Nos. 11774167 and 61571222), Fundamental Research Funds for the Central Universities, China (Grant No. 020414380001), State Key Laboratory of Acoustics, Chinese Academy of Sciences (Grant No. SKLA201609), and AQSIQ Technology R & D Program, China (Grant No. 2017QK125).

†Corresponding author. E-mail: xzliu@nju.edu.cn

© 2018 Chinese Physical Society and IOP Publishing Ltd

two-dimensional (2D) finite beams, therefore, here the two AiG beams and the cylindrical particle are both considered to be two-dimensional. The results displayed may contribute to the developments of cell screening, drug delivery, and the design of the acoustic tweezers.

2. Theory

Two incident Airy–Gaussian beams propagating along the x axis at normal incidence with respect to the z axis of a cylindrical particle are considered here, as shown in Fig. 1. Omitting the time harmonic factor $\exp(-\mathrm{i}\omega t)$ in all expressions for convenience, the initial profile of the incident velocity potential field for the two AiG beams is

$$\begin{aligned}\Phi_{\mathrm{i}}^{(0)}(x=0,y) &= \phi_0 \mathrm{Ai}\left(\frac{y}{y_0}\right)\mathrm{e}^{\alpha(y/y_0)}\mathrm{e}^{-(y/w_0)^2} \\ &\quad + \phi_0 \mathrm{e}^{\mathrm{i}Q}\mathrm{Ai}\left(\frac{-y}{y_0}\right)\mathrm{e}^{\alpha(-y/y_0)}\mathrm{e}^{-(-y/w_0)^2}, \quad (1)\end{aligned}$$

where ϕ_0 is the amplitude of the incident velocity potential of the two AiG beams; $\mathrm{Ai}(x)$ is the Airy function; y_0 is the arbitrary transverse scale; α is the decaying parameter; Q is the phase difference between the two AiG beams; and w_0 is the beam width. Based on the angular spectrum decomposition in plane waves,[25] the incident velocity potential in the Cartesian coordinate system can be expressed as

$$\Phi_{\mathrm{i}}(x,y) = \int_{-\infty}^{\infty} g(p,q)\,\mathrm{e}^{\mathrm{i}k(px+qy)}\mathrm{d}q, \quad (2)$$

where k is the wavenumber, (p,q) are the propagation direction of the plane wave components and $p=\cos\beta, q=\sin\beta$, with β the propagation angle. $g(p,q)$ is the angular spectrum function which is determined by the initial profile of the incident velocity potential field and can be obtained by the inverse Fourier transform

$$g(p,q) = \frac{1}{\lambda}\int_{-\infty}^{\infty}\Phi_{\mathrm{i}}^{(0)}(x=0,y)\,\mathrm{e}^{-\mathrm{i}k(px+qy)}\mathrm{d}y, \quad (3)$$

where λ is the wavelength. Substituting Eq. (1) into Eq. (3) and applying the Airy transformation formula,[26] we can obtain the angular spectrum function

$$\begin{aligned}g(p,q) &= \phi_0\frac{ky_0}{2\pi}\frac{\sqrt{\pi}}{\chi} \\ &\quad\times\left[\mathrm{e}^{(\frac{\alpha-\mathrm{i}kqy_0}{2\chi})^2}\mathrm{e}^{\frac{\alpha-\mathrm{i}kqy_0}{8\chi^4}+\frac{1}{96\chi^6}}\mathrm{Ai}\left(\frac{\alpha-\mathrm{i}kqy_0}{2\chi^2}+\frac{1}{16\chi^4}\right)\right. \\ &\quad -\mathrm{e}^{\mathrm{i}Q}\mathrm{e}^{(\frac{\alpha+\mathrm{i}kqy_0}{2\chi})^2}\mathrm{e}^{\frac{\alpha+\mathrm{i}kqy_0}{8\chi^4}+\frac{1}{96\chi^6}} \\ &\quad\left.\times\mathrm{Ai}\left(\frac{\alpha+\mathrm{i}kqy_0}{2\chi^2}+\frac{1}{16\chi^4}\right)\right], \quad (4)\end{aligned}$$

where $\chi = y_0/w_0$, and ky_0 is a dimensionless transverse scale. By substituting Eq. (4) into Eq. (2), the incident velocity potential can be written as

$$\begin{aligned}\Phi_{\mathrm{i}}(x,y) &= \phi_0\frac{ky_0}{2\pi}\frac{\sqrt{\pi}}{\chi}\mathrm{e}^{\frac{1}{96\chi^6}} \\ &\quad\times\left[\int_{-\infty}^{\infty}\mathrm{e}^{(\frac{\alpha-\mathrm{i}kqy_0}{2\chi})^2+\frac{\alpha-\mathrm{i}kqy_0}{8\chi^4}}\right. \\ &\quad\times\mathrm{Ai}\left(\frac{\alpha-\mathrm{i}kqy_0}{2\chi^2}+\frac{1}{16\chi^4}\right)\mathrm{e}^{\mathrm{i}k(px+qy)}\mathrm{d}q \\ &\quad -\mathrm{e}^{\mathrm{i}Q}\int_{-\infty}^{\infty}\mathrm{e}^{(\frac{\alpha+\mathrm{i}kqy_0}{2\chi})^2+\frac{\alpha+\mathrm{i}kqy_0}{8\chi^4}} \\ &\quad\left.\times\mathrm{Ai}\left(\frac{\alpha+\mathrm{i}kqy_0}{2\chi^2}+\frac{1}{16\chi^4}\right)\mathrm{e}^{\mathrm{i}k(px+qy)}\mathrm{d}q\right]. \quad (5)\end{aligned}$$

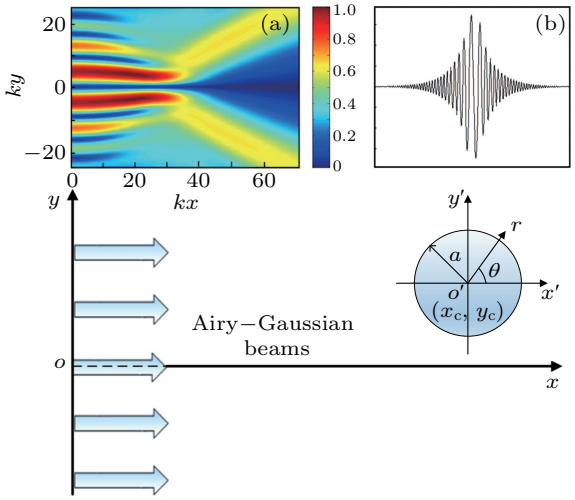


Fig. 1. Schematic diagram of two Airy–Gaussian beams interacting with a cylindrical particle. The two beams propagate along the x direction, and the particle is located in the Cartesian coordinate system x'–o'–y'. a and (x_c, y_c) are the radius and the center of the particle, respectively. Insets (a) and (b) show the incident velocity potential and the incident profile of the two Airy–Gaussian beams with the phase difference $Q=0$, respectively.

By applying the Jacobi–Anger expansion,[27] equation (5) can be rewritten in the cylindrical coordinate system as

$$\Phi_{\mathrm{i}}(r,\theta) = \phi_0\sum_{n=-\infty}^{\infty}\mathrm{J}_n(kr)\,\mathrm{e}^{\mathrm{i}n\theta}\Lambda_n, \quad (6)$$

where $\mathrm{J}_n(\cdot)$ is the n-th order Bessel function, and Λ_n is the beam shape coefficient

$$\Lambda_n = \frac{ky_0}{2\pi}\frac{\sqrt{\pi}}{\chi}\mathrm{e}^{\frac{1}{96\chi^6}}\mathrm{i}^n(a_n-b_n), \quad (7)$$

with

$$\begin{aligned}a_n &= \int_{-\infty}^{\infty}\mathrm{e}^{(\frac{\alpha-\mathrm{i}kqy_0}{2\chi})^2+\frac{\alpha-\mathrm{i}kqy_0}{8\chi^4}}\mathrm{e}^{\left(x_c\sqrt{1-q^2}+y_cq\right)} \\ &\quad\times\mathrm{Ai}\left(\frac{\alpha-\mathrm{i}kqy_0}{2\chi^2}+\frac{1}{16\chi^4}\right)\mathrm{e}^{-\mathrm{i}n\sin^{-1}q}\mathrm{d}q, \\ b_n &= \mathrm{e}^{\mathrm{i}Q}\int_{-\infty}^{\infty}\mathrm{e}^{(\frac{\alpha+\mathrm{i}kqy_0}{2\chi})^2+\frac{\alpha+\mathrm{i}kqy_0}{8\chi^4}}\mathrm{e}^{\left(x_c\sqrt{1-q^2}+y_cq\right)}\end{aligned}$$

$$\times \mathrm{Ai}\left(\frac{\alpha+\mathrm{i}kqy_0}{2\chi^2}+\frac{1}{16\chi^4}\right)\mathrm{e}^{-\mathrm{i}n\sin^{-1}q}\mathrm{d}q.$$

The scattering velocity potential produced by the cylindrical particle can be expressed as

$$\Phi_{\mathrm{s}}(r,\theta)=\sum_{n=-\infty}^{\infty}s_n\mathrm{H}_n^{(1)}(kr)\,\mathrm{e}^{\mathrm{i}n\theta}\Lambda_n, \tag{8}$$

where s_n are the scattering coefficients determined by the boundary condition at the surface of the cylindrical particle, which means the continuity of stresses and displacements. Also, $\mathrm{H}_n^{(1)}(\cdot)$ is the n-th Hankel function of first order.

Based on the incident and scattering velocity potentials, the longitudinal (along the x axis) and transverse (along the y axis) radiation force functions can be obtained respectively as follows:[28]

$$Y_x=\frac{1}{ka}\Im\left\{\sum_{n=-\infty}^{\infty}\Lambda_n(1+s_n)\left[\Lambda_{n+1}^*s_{n+1}^*-\Lambda_{n-1}^*s_{n-1}^*\right]\right\}, \tag{9}$$

$$Y_y=-\frac{1}{ka}\Re\left\{\sum_{n=-\infty}^{\infty}\Lambda_n(1+s_n)\left[\Lambda_{n+1}^*s_{n+1}^*+\Lambda_{n-1}^*s_{n-1}^*\right]\right\}, \tag{10}$$

where a is the radius of the cylindrical particle, the superscript * denotes the conjugate of a complex number.

3. Simulation and discussion

This section presents several simulation results of the radiation force functions for two AiG beams. The material of the cylindrical particle used in the simulation is Lucite (with the density $\rho_1=1191$ kg/m^3, compressional velocity $c_1=2690$ m/s, shear velocity $c_2=1340$ m/s, normalized longitudinal absorption $\gamma_1=0.0035$, and normalized shear absorption $\gamma_2=0.0053$[29]) and the host fluid is water ($\rho_0=1000$ kg/m^3, $c_0=1500$ m/s). In the following numerical simulation, we take $ky_0=4$ and $\alpha=0.01$.

Figure 2 shows the acoustic radiation force function vector field $\boldsymbol{Y}_\perp=Y_x\boldsymbol{e}_x+Y_y\boldsymbol{e}_y$ denoted by the vector arrows and the motion trajectories of the cylindrical particle induced by the two AiG beams with different phases. Here we take four kinds of phases $Q=0,\pi/2,\pi,3\pi/2$ and $ka=0.1$, $w_0=\lambda$ in the simulation. From Fig. 2, we can find that the radiation force function vectors distribute symmetrically along the x axis in Figs. 2(a) and 2(c), and the forces near both sides of the x axis can pull the particle back to the x axis when $Q=0$, in contrast the forces near both sides of the x axis will push the particle away from the x axis when $Q=\pi$. Also, when $Q=\pi/2,3\pi/2$, most of the force function vectors give the forces which will push the particle away from the x axis, as shown in Figs. 2(b) and 2(d). In addition, the force function vectors distribute asymmetrically along the x axis when $Q=\pi/2,\ 3\pi/2$. If we reverse the force function vector along the x axis when $Q=\pi/2$, it is interesting to find that the reversed force function vector is the same as that when $Q=3\pi/2$.

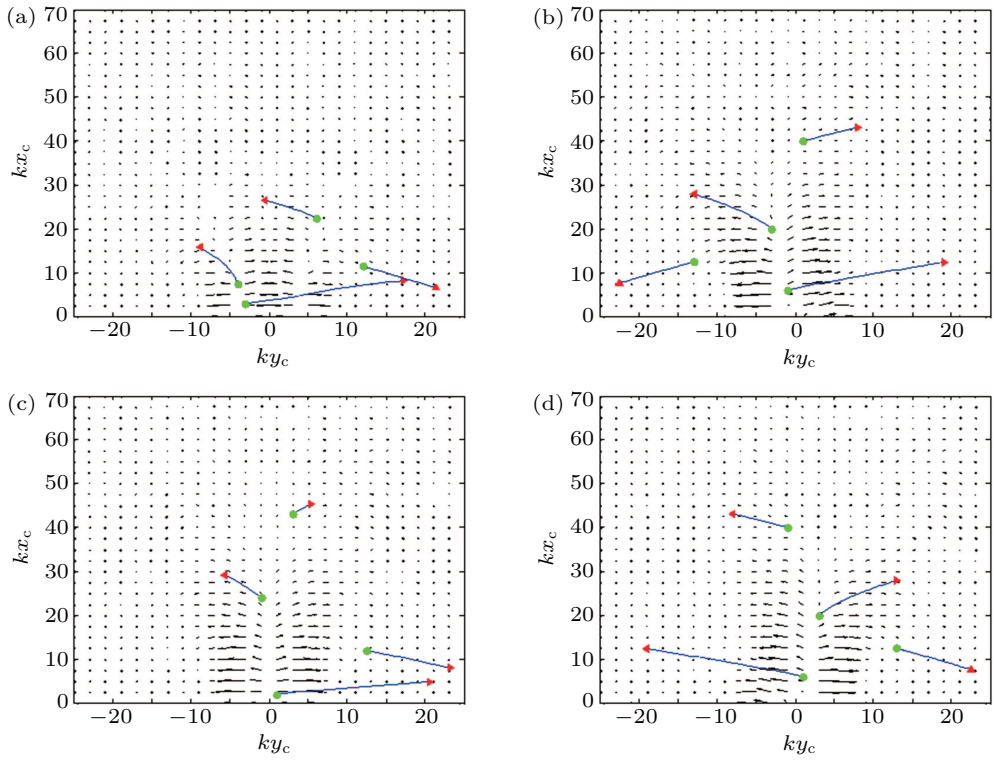


Fig. 2. The acoustic radiation force function vector field and the motion trajectories of the cylindrical particle for different phases: (a) $Q=0$, (b) $Q=\pi/2$, (c) $Q=\pi$, (d) $Q=3\pi/2$.

The computation of the motion trajectories of the cylindrical particle, only determined by the acoustic radiation force and the viscous drag force in the x–y plane here, is based on Newton's second law of motion which is expressed as

$$m\boldsymbol{r}'' = \boldsymbol{F}_{\rm rad} + \boldsymbol{F}_{\rm drag}, \tag{11}$$

where m is the mass of the particle, $\boldsymbol{r}'' = {\rm d}^2\boldsymbol{r}/{\rm d}t^2$ is the acceleration, t is the time in units of second, $\boldsymbol{F}_{\rm rad}(=\boldsymbol{Y}_{\perp}S_{\rm c}E_0)$ is the acoustic radiation force vector, and $\boldsymbol{F}_{\rm drag}(=-32\eta a\boldsymbol{r}'/3)$ is the viscous drag force vector. Here $S_{\rm c}(=2al)$ is the cross-sectional area of the cylindrical particle, $E_0(=1/2\rho_0 k^2\,|\phi_0|^2)$ is a characteristic energy density, $\eta\,(=0.001\ {\rm Pa}\cdot{\rm s})$ is the dynamic viscosity, and $\boldsymbol{r}' = {\rm d}\boldsymbol{r}/{\rm d}t$ is the velocity.

The computation of the motion trajectories of the particle in MATLAB is accomplished by using the step-iterative Runge–Kutta method, the position and the velocity of the particle at the next time-step can be determined from the values at the previous time-step. In the simulations, the initial vector velocity and the initial time are all set to be zero, and the beam intensity is set to be $3.3\times10^8\ {\rm W/m^2}$. There are four motion trajectories of the particle shown in Figs. 2(a)–2(d), where the green circle represents the initial position and the red triangle represents the end position of the particle. From Fig. 2, we can find that the cylindrical particle can be pushed away from the y axis or pulled back towards the y axis along a curved trajectory from the initial position under the effect of the acoustic radiation force. The particle's trajectory becomes longer when it passes through the area with bigger acoustic radiation force. Three of four motion trajectories show that the particle is propelled away from y axis in Figs. 2(a)–2(d), specifically, there is one trajectory showing that the particle is dragged back towards the y axis, those special initial positions of the particle are $(kx_{\rm c}, ky_{\rm c}) = (11.5, 6), (12.5, -13), (12, 12.5)$, and $(12.5, 13)$ in Figs. 2(a)–2(d), respectively. Besides, the initial positions of the cylindrical particle in Fig. 2(b) are symmetric with those in Fig. 2(d) about the x axis and we can find that their trajectories are also symmetric about the x axis, which is in agreement with the previous result that the reversed force function vector at $Q=\pi/2$ is the same as that at $Q=3\pi/2$.

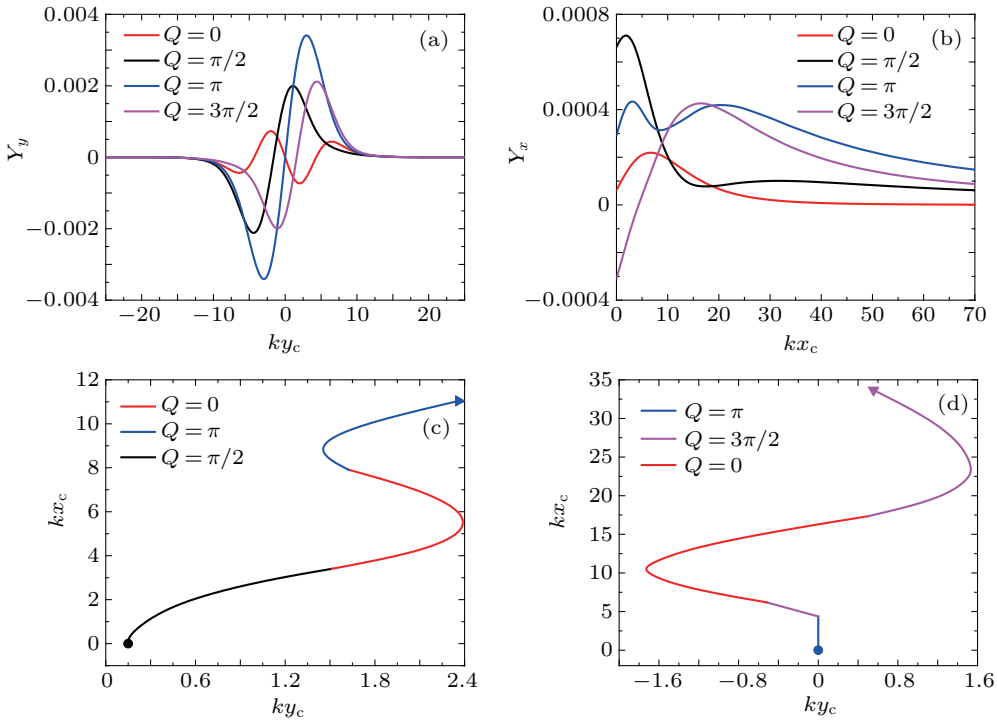


Fig. 3. The radiation force functions and the motion trajectories of the particle for different phases. (a) The transverse forces when $kx_{\rm c}=10$. (b) The longitudinal forces when $ky_{\rm c}=3$. (c) and (d) The motion trajectories of the particle under the effect of the varied phases.

Figure 3 shows the radiation force functions and the motion trajectories of the particle with different phases, here we take $ka=0.1$ and $w_0=\lambda$ in the simulation. Figure 3(a) describes the transverse forces with different phases on the particle when $kx_{\rm c}$=10, where we can find that there are positive and negative transverse forces which can pull or push the particle into either the positive or the negative y direction. Meanwhile, the longitudinal forces shown in Fig. 3(b) when $ky_{\rm c}=3$ are nearly all positive, which can just push the particle along the positive x direction. Figures 3(c) and 3(d) show that the motion trajectories of the particle change with the varied phases, where the circle represents the initial position and the trian-

gle represents the end position of the particle. In Fig. 3(c), the particle keeps moving upward, meanwhile, it firstly accelerates toward the positive y direction under the effect of the force function vector at $Q=\pi/2$, then decelerates until it turns to the opposite direction after Q is converted into 0 from $\pi/2$, after that the particle is dragged back to the positive y direction again by converting the phase $Q=0$ into $Q=\pi$. Similarly, the particle is pushed or pulled into either the positive or the negative y direction by changing the phase, meanwhile, the particle is still moving upward, as shown in Fig. 3(d). Observing the motion trajectories of the particle and the radiation force functions changing with the phases in Fig. 3, we can find that the direction of the particle can be changed in the y direction by controlling the phase, which means that it is the transverse acoustic radiation force that plays an important role in changing the direction of the particle.

Next we investigate the influence of the beam width on the radiation force function. Here we take the phase $Q=0$ with different beam widths as examples. The background of Fig. 4(a) is the incident regularized normalized intensity field ratio (I/I_0) of two AiG beams at $w_0=\lambda$, where $I_0=\rho_0 w^2|\phi_0|^2/(2c_0)$, over which the superimposed plot is the force function vector $\boldsymbol{Y}_\perp$ denoted by the vector arrow. Figure 4(c) describes the same as Fig. 4(a) but at $w_0=4\lambda$. The transverse radiation force functions with $w_0=\lambda$ and $w_0=4\lambda$ are shown in Figs. 4(b) and 4(d), respectively. It is found that that when the beam width w_0 decreases, the intensity distribution is simpler with fewer side lobes, which results from the interception effect of the Gaussian factor on the two AiG beams. The larger w_0 is, the more complex and the bigger the transverse acoustic radiation force is, just like the intensity distribution, because the acoustic radiation force is closely connected to the intensity.

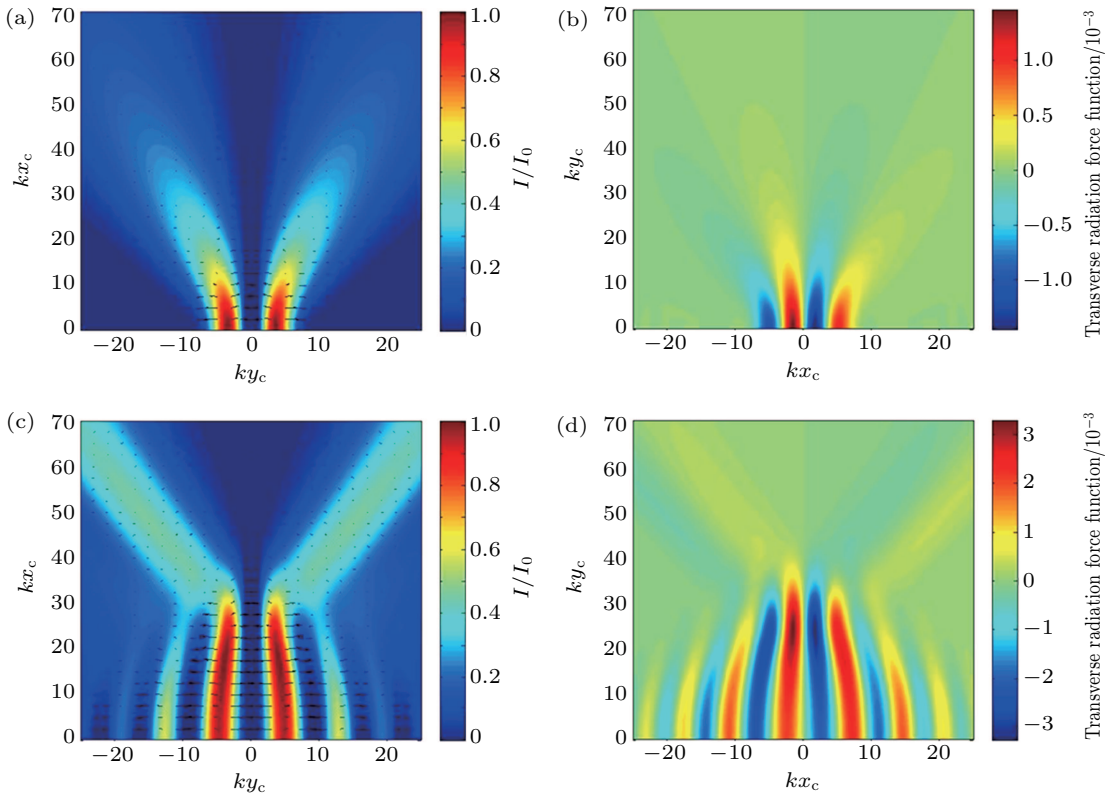


Fig. 4. The backgrounds of panels (a) and (c) describe the incident regularized normalized intensity field ratio (I/I_0) of two AiG beams, over which the force function vectors are superimposed; panels (b) and (d) show the transverse radiation force functions. In panels (a) and (b), $w_0=\lambda$; in panels (c) and (d), $w_0=4\lambda$.

Figure 5 shows the effect of the dimensionless frequency bandwidth on the radiation force functions. Here we take $w_0=\lambda$ and the initial position of the particle is $(kx_c, ky_c)=(0,-3)$. Figures 5(a)–5(d) describe the longitudinal and transverse radiation force functions at $Q=0,\pi/2,\pi,3\pi/2$, respectively. As we can see from Fig. 5, the transverse radiation forces can be positive or negative over the dimensionless frequency bandwidth $0\le ka\le 10$, however, the longitudinal radiation force is always positive and grows more rapidly than the transverse force when $ka>1$, and both of their amplitudes tend to be constant after several peaks and valleys. Positive and negative transverse forces can always be obtained by choosing the appropriate phase when $0\le ka\le 5$, which means that we can pull or push the particle into either the positive or negative transverse direction by turning the phase appropriately.

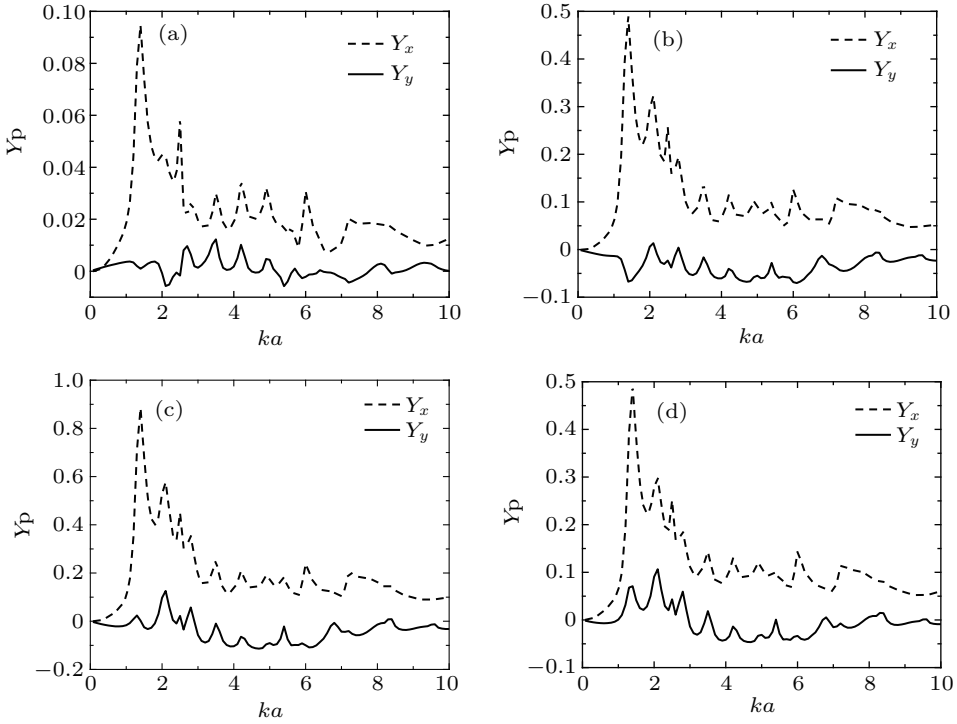


Fig. 5. The radiation force functions of the cylindrical particle at $(kx_c, ky_c) = (0, -3)$ changing with ka at different phases: (a) $Q = 0$, (b) $Q = \pi/2$, (c) $Q = \pi$, (d) $Q = 3\pi/2$.

4. Conclusion

In summary, we obtain the radiation force of two AiG beams on a cylindrical particle by using the angular spectrum decomposition and partial-wave series expansion methods and simulate the corresponding force functions and the motion trajectories of the particle with different parameters. We notice that the transverse direction of the accelerated particle can be controlled by turning the phase Q; the radiation forces become bigger and the distributions of the force become more complex when the beam width w_0 increases; the control of the particle's direction in the transverse direction can be achieved over a large frequency bandwidth range, which means we can find appropriate ka to manipulate the particle in experiments by adjusting the frequency. This work may provide a method to deliver particles to a target location by choosing suitable phases of two AiG beams and may contribute to the development for the design of acoustical tweezers.

References

[1] Mitri F G 2005 *Eur. Phys. J. B* **43** 379
[2] Mitri F G 2006 *New J. Phys.* **8** 138
[3] Wu R R, Cheng K X, Liu X Z, Liu J H and Gong X F 2016 *Wave Motion* **62** 63
[4] Zhang X F, Yun Q, Zhang Q B and Sun X N 2016 *Acta Acust. United Ac.* **102** 334
[5] Silva G T and Baggio A L 2015 *Ultrasonics* **56** 449
[6] Mitri F G 2015 *Wave Motion* **57** 231
[7] Marston P L 2007 *J. Acoust. Soc. Am.* **122** 3162
[8] Berry M V and Balazs N L 1979 *Am. J. Phys.* **47** 264
[9] Unnikrisnan K and Rau A R P 1996 *Am. J. Phys.* **64** 1034
[10] Omori R, Kobayashi T and Suzuki A 1997 *Opt. Lett.* **22** 816
[11] Ashkin A, Dziedzic J M, Bjorkholm J E and Chu S 1986 *Opt. Lett.* **11** 288
[12] Jiang Y F, Huang K K and Lu X H 2013 *Opt. Express* **21** 24413
[13] Zhao Z Y, Zang W P and Tian J G 2016 *J. Opt.* **18** 025607
[14] Mitri F G 2017 *Appl. Phys. Lett.* **110** 091104
[15] Mitri F G 2016 *J. Appl. Phys.* **120** 104901
[16] Bandres M A and Gutierrez-vega J C 2007 *Opt. Express* **15** 16719
[17] Siviloglou G A and Christodoulides D N 2007 *Opt. Lett.* **32** 979
[18] Huang J Y, Liang Z J, Deng F, Yu W H, Zhao R H, Chen B, Yang X B and Deng D M 2015 *J. Opt. Soc. Am. A* **32** 2104
[19] Deng D M 2011 *Eur. Phys. J. D* **65** 553
[20] Zhou M L, Chen C D, Chen B, Peng X, Peng Y L and Deng D M 2015 *Chin. Phys. B* **24** 124102
[21] Chen C D, Chen B, Peng X and Deng D M 2015 *J. Opt.* **17** 035504
[22] Peng Y L, Peng X, Chen B, Zhou M L, Chen C D and Deng D M 2016 *Opt. Commun.* **359** 116
[23] Zhang X P 2016 *Opt. Commun.* **367** 364
[24] Mitri F G 2016 *J. Appl. Phys.* **120** 144902
[25] Goodman J W 1968 *Introduction to Fourier Optics* (New York: McGraw-Hill) pp. 55–62
[26] Vallee O and Soares M 2004 *Airy Functions and Applications to Physics* (London: World Scientific) pp. 74–84
[27] Colton D and Kress R 2013 *Inverse Acoustic and Electromagnetic Scattering Theory* (3rd Edn.) (New York: Springer Science + Business Media) p. 33
[28] Mitri F G 2015 *Ultrasionics* **62** 244
[29] Mitri F G 2005 *Eur. Phys. J. B* **44** 71